ELSEVIER

Comput. Methods Appl. Mech. Engrg. 183 (2000) 87–103

Computer methods in applied mechanics and engineering

www.elsevier.com/locate/cma

An anisotropic gradient damage model for quasi-brittle materials

Ellen Kuhl [a], Ekkehard Ramm [a], René de Borst [b,*]

[a] *Institute of Structural Mechanics, University of Stuttgart, 70550 Stuttgart, Germany*
[b] *Koiter Institute Delft/Faculty of Aerospace Engineering, TU Delft, P.O. Box 5058, 2600 GB Delft, The Netherlands*

Received 6 April 1998

Abstract

An anisotropic continuum damage model based on the microplane concept is elaborated. Scalar damage laws are formulated on several individual microplanes representing the planes of potential failure. These uniaxial constitutive laws can be cast into a fourth-order damage formulation such that anisotropy of the overall constitutive law is introduced in a natural fashion. Strain gradients are incorporated in the constitutive equations in order to account for microstructural interaction. Consequently, the underlying boundary value problem remains well-posed even in the softening regime. The gradient continuum enhancement results in a set of additional partial differential equations which are satisfied in a weak form. Additional nodal degrees of freedom are introduced which leads to a modified element formulation. The governing equations can be linearized consistently and solved within an incremental-iterative Newton–Raphson solution procedure. The capability of the present model to properly simulate the localized failure of quasi-brittle materials will be demonstrated by means of several examples.

1. Introduction

The failure mechanism of heterogeneous materials is of a complex nature. Microcracks tend to develop at the weakest part of the material leading to failure induced anisotropy. Considering concrete for example, microcracking usually starts at the interface between the stiff grains and the cement matrix. Growth and coalescence of these microcracks result in a global stiffness degradation and a typical localized failure pattern.

Beyond a certain level of accumulated damage, stiffness degradation accompanied by strain softening may result in loss of well-posedness of the boundary value problem. This deficiency of classical continua can be avoided by the introduction of an internal length scale. Several techniques to incorporate an internal length have been suggested such as Cosserat continua, nonlocal continuum models or the inclusion of viscous terms. Herein, we will apply a nonlocal enhancement of the continuum model. Physically, the introduction of nonlocal terms can be interpreted by taking into account the heterogeneous substructure of the material leading to characteristic long range mechanisms such as dislocation motion in metal plasticity, e.g., Aifantis [1], or microcrack interaction in materials like concrete, see Bažant [6]. Since classical continua are unable to describe this interaction at the material point level, the enhancement of the continuum model by nonlocal terms, either introduced through an integral equation, or through an additional gradient equation has become popular. The incorporation of nonlocal quantities through integral equations has already been proposed in the late 1960s by Kröner [16] as well as by Eringen and Edelen [13] for elastic

* Corresponding author.
E-mail address: R.deBorst@lr.TUDelft.nl (R. de Borst).

0045-7825/00/$ - see front matter
PII: S0045-7825(99)00213-3

material models. Later, their ideas have been extended to continuum damage mechanics by Pijaudier-Cabot and Bažant [3,25]. Either the energy release rate or the damage variable itself were introduced as the scalar valued nonlocal quantity. Nonlocal anisotropic damage formulations based on a tensorial nonlocal variable, namely the strain field, have also been discussed, see Bažant and Ožbolt [5]. However, the application of nonlocal integral models is not efficient from a computational point of view. A global averaging procedure is required and the resulting equations cannot be linearized easily, see Peerlings et al. [23]. Consequently, nonlocal integral models are not considered promising for large scale computations.

An elegant alternative to the nonlocal integral equation was proposed among others by Lasry and Belytschko [18] and by Mühlhaus and Aifantis [20]. In their gradient continuum models, nonlocality is incorporated through a gradient term. An additional equation ensues, which is usually fulfilled in a weak sense and the nonlocal quantity is introduced as independent variable. The constitutive equations thus remain local in a finite element sense and the linearization is straightforward. The introduction of gradients in combination with softening plasticity models is now well established, see Mühlhaus and Aifantis [20], de Borst and Mühlhaus [7] and Pamin [21] among others. In gradient plasticity models, the gradient term is usually introduced into the constitutive equations through the yield function. The application of gradients in combination with continuum damage mechanics has been presented recently by Peerlings et al. [22] in the context of isotropic damage evolution. Again, the equivalent strain, see Peerlings et al. [24], or the damage variable itself, see de Borst et al. [9], can be chosen as the nonlocal quantity. The application of a gradient continuum enhancement to anisotropic damage evolution has not been analyzed hitherto, and is the scope of this study.

The general idea of modelling anisotropy by considering the material behavior on several independent planes goes back to the early ideas of Taylor [28], which were motivated by the crystallographic slip on several independent slip planes. This reduction to scalar constitutive laws formulated on potential failure planes was modified by Bažant and Gambarova [2] who introduced the so-called microplane model in the context of the quasi-brittle failure of concrete. The original model has been enhanced by Bažant and Prat [4], Carol et al. [11] and recently by Kuhl and Ramm [17]. The stiffness degradation on the individual microplanes is described by the concept of continuum damage mechanics, see e.g., Kachanov [15], Lemaitre and Chaboche [19] and Simo and Ju [26]. Including different uniaxial constitutive laws for tension, compression and shear, the model takes into account mode I as well as mode II failure in a natural fashion. In analogy to the theory of plasticity, the evolution of damage is governed by damage loading functions. Strain gradients are introduced in the individual loading functions to avoid the loss of well-posedness in the post-critical regime.

The paper is organized as follows. After introducing the enhancement of the continuum by gradient terms, we will briefly summarize the constitutive equations of the microplane model. The influence of the strain gradient term on the microplane equations will be elaborated. Afterwards, the finite element implementation of the gradient enhanced microplane model will be derived. Finally, some examples will be given to demonstrate the features of the model by simulating the complex failure mechanisms of quasi-brittle materials.

2. Gradient enhanced continuum model

2.1. Nonlocal continuum models

In the following, we will present the general concept of nonlocal contina from which we will derive the gradient continuum enhancement as a special case. Motivated by the long-range microstructural interaction, the stress response $\boldsymbol{\sigma}$ of a material point is assumed to depend not only on the state of the point itself, but also on the state of its neighborhood. Based on the early nonlocal elasticity models by Kröner [16] and Eringen and Edelen [13], the definition of any nonlocal quantity $\bar{\boldsymbol{Y}}$ can be expressed as the weighted average of its local counterpart $\boldsymbol{Y}$ over a surrounding volume V:

$$\bar{\boldsymbol{Y}} = \frac{1}{V} \int_V g(\boldsymbol{\xi})\, \boldsymbol{Y}(\boldsymbol{x}+\boldsymbol{\xi})\, \mathrm{d}V. \tag{1}$$

Herein, $g(\xi)$ represents a certain weight function, which decays smoothly with the distance, for example the Gaussian distribution function

$$g(\xi) = \frac{1}{2\pi l^2} \exp\left[\frac{-\xi^2}{2l^2}\right] \quad \text{with} \quad \frac{1}{V}\int_V g(\xi)\, \mathrm{d}V = 1. \tag{2}$$

The extent of the long-range interaction is governed by the internal length scale parameter l. The distance from the point $\boldsymbol{x}$ to a point in its neighborhood is denoted by $\boldsymbol{\xi}$. For isotropic material behavior, it is in general sufficient to apply the averaging equation (1) to a scalar-valued quantity, for example the equivalent strain or the damage variable. For anisotropic models, which are the scope of this study, the nonlocal generalization should be applied to a tensorial quantity.

2.2. Introduction of strain gradients

In the following, the averaging equation (1) will be applied to the strain tensor $\boldsymbol{\epsilon}$, leading to the definition of its nonlocal counterpart $\bar{\boldsymbol{\epsilon}}$ of the following form:

$$\bar{\boldsymbol{\epsilon}} = \frac{1}{V}\int_V g(\xi)\boldsymbol{\epsilon}(\boldsymbol{x}+\xi)\, \mathrm{d}V. \tag{3}$$

According to Lasry and Belytschko [18] and Mühlhaus and Aifantis [20], this nonlocal integral equation can be approximated by a partial differential equation. Therefore, we replace the local strain tensor of Eq. (3) by its Taylor expansion at $\boldsymbol{\xi} = \boldsymbol{0}$:

$$\boldsymbol{\epsilon}(\boldsymbol{x},\xi) = \boldsymbol{\epsilon}(\boldsymbol{x}) + \nabla\boldsymbol{\epsilon}(\boldsymbol{x})\xi + \frac{1}{2!}\nabla^{(2)}\boldsymbol{\epsilon}(\boldsymbol{x})\xi^{(2)} + \frac{1}{3!}\nabla^{(3)}\boldsymbol{\epsilon}(\boldsymbol{x})\xi^{(3)} + \frac{1}{4!}\nabla^{(4)}\boldsymbol{\epsilon}(\boldsymbol{x})\xi^{(4)} + \cdots \tag{4}$$

Herein, $\nabla^{(i)}$ denotes the ith order gradient operator. The combination of Eqs. (3) and (4) yields the following definition of the nonlocal strain tensor:

$$\begin{aligned}\bar{\boldsymbol{\epsilon}} = {} & \frac{1}{V}\int_V g(\xi)\boldsymbol{\epsilon}(\boldsymbol{x})\, \mathrm{d}V + \frac{1}{V}\int_V g(\xi)\nabla\boldsymbol{\epsilon}(\boldsymbol{x})\xi\, \mathrm{d}V + \frac{1}{2!V}\int_V g(\xi)\nabla^{(2)}\boldsymbol{\epsilon}(\boldsymbol{x})\xi^2\, \mathrm{d}V \\ & + \frac{1}{3!V}\int_V g(\xi)\nabla^{(3)}\boldsymbol{\epsilon}(\boldsymbol{x})\xi^3\, \mathrm{d}V + \frac{1}{4!V}\int_V g(\xi)\nabla^{(4)}\boldsymbol{\epsilon}(\boldsymbol{x})\xi^4\, \mathrm{d}V + \cdots\end{aligned} \tag{5}$$

With the assumption of an isotropic influence of the averaging equation, the integrals of the odd terms vanish. Truncating the Taylor series of Eq. (4) after the quadratic term leads to the following definition of the nonlocal strain tensor:

$$\bar{\boldsymbol{\epsilon}} = \frac{1}{V}\int_V g(\xi)\boldsymbol{\epsilon}(\boldsymbol{x})\, \mathrm{d}V + \frac{1}{2!V}\int_V g(\xi)\nabla^{(2)}\boldsymbol{\epsilon}(\boldsymbol{x})\xi^2\, \mathrm{d}V, \tag{6}$$

which can be transformed into the partial differential equation given below

$$\bar{\boldsymbol{\epsilon}} = \boldsymbol{\epsilon} + c\nabla^2\boldsymbol{\epsilon}. \tag{7}$$

Herein, the constant c is proportional to a length squared. For sake of simplicity, we will apply only *one* constant c, thus weighting each component of the gradient term identically. Nevertheless, for the case of anisotropic damage evolution, an extension to a different weighting of the individual coefficients, which results in several different integration constants c_{11}, c_{22}, c_{12}, etc., is straightforward. The gradient parameter c can be replaced by a varying quantity depending on the load history as proposed by Geers [14]. Nevertheless, within this contribution we will adopt a constant gradient model. When embedding Eq. (7) in a finite element analysis, the discretized displacement field $\boldsymbol{u}$ has to fulfill $\mathscr{C}^1$ continuity requirements. Similar to Peerlings et al. [22], we will therefore approximate Eq. (7) by the following expression:

$$\boldsymbol{\epsilon} = \bar{\boldsymbol{\epsilon}} - c\nabla^2\bar{\boldsymbol{\epsilon}} \tag{8}$$

which is still of second-order accuracy, but requiring only a $\mathscr{C}^0$ continuous displacement approximation. In order to solve the averaging partial differential Eq. (8), additional boundary conditions, either of the Dirichlet or of the Neumann type,

$$\bar{\boldsymbol{\epsilon}} = \bar{\boldsymbol{\epsilon}}^p \quad \text{or} \quad \nabla\bar{\boldsymbol{\epsilon}} \cdot \boldsymbol{n} = \bar{\boldsymbol{\epsilon}}^p_n \quad \text{on } \Gamma \tag{9}$$

become necessary. The issue of additional boundary conditions has been discussed in detail by Lasry and Belytschko [18] as well as by Mühlhaus and Aifantis [20]. Herein, we will adopt the natural boundary condition of a vanishing gradient

$$\nabla\bar{\boldsymbol{\epsilon}} \cdot \boldsymbol{n} = \boldsymbol{0} \tag{10}$$

at every point of the boundary. Nevertheless, the physical interpretation of the additional boundary condition is still an unsolved issue.

3. Anisotropic damage model

The following anisotropic damage description is based on the ideas of the microplane model as described in detail by Bažant and Prat [4] or more recently by Carol and Bažant [12]. The original microplane model developed for materials like concrete is motivated by the idea of modelling discrete potential failure planes. Physically, these planes can be interpreted as the weakest material planes, represented by the interface between the grains and the cement matrix. Herein, we apply a kinematically constrained microplane model, based on the projection of the overall strain tensor $\boldsymbol{\epsilon}$ onto the individual planes, the plane-wise formulation of uniaxial damage laws and, finally, a homogenization procedure to determine the overall stress tensor $\boldsymbol{\sigma}$. After briefly summarizing the derivation of the overall constitutive law, its modification due to the additional gradient term will be illustrated.

3.1. Microplane kinematics

Restricting the constitutive model to small strains, the macroscopic strain tensor $\boldsymbol{\epsilon}$ is given as the symmetric part of the displacement gradient $\nabla\boldsymbol{u}$:

$$\boldsymbol{\epsilon} = \nabla^{\text{sym}}\boldsymbol{u}. \tag{11}$$

The microplane model developed for concrete distinguishes between normal volumetric, normal deviatoric and tangential material behavior. We therefore calculate the scalar-valued volumetric and deviatoric strain components for every individual microplane I, namely ϵ_{V} and ϵ^I_{D}, and the components R of the tangential strain vector ϵ^{RI}_{T}, by projecting the macroscopic strain tensor $\boldsymbol{\epsilon}$ onto the material planes:

$$\epsilon_{\text{V}} = \boldsymbol{\epsilon} : \boldsymbol{V}, \qquad \epsilon^I_{\text{D}} = \boldsymbol{\epsilon} : \boldsymbol{D}^I, \qquad \epsilon^{RI}_{\text{T}} = \boldsymbol{\epsilon} : \boldsymbol{T}^{RI}. \tag{12}$$

The individual projection tensors $\boldsymbol{V}$, $\boldsymbol{D}^I$ and $\boldsymbol{T}^{RI}$ are defined by the geometry of each microplane in terms of the $\boldsymbol{n}^I$, the normal to the Ith plane see Fig. 1:

$$\begin{aligned} \boldsymbol{V} &:= \frac{1}{3}\boldsymbol{1}, \\ \boldsymbol{D}^I &:= \boldsymbol{n}^I \otimes \boldsymbol{n}^I - \frac{1}{3}\boldsymbol{1}, \\ \boldsymbol{T}^{RI} &:= \frac{1}{2}\left(\boldsymbol{n}^I_J 1_{KR} + \boldsymbol{n}^I_K 1_{JR} - 2\boldsymbol{n}^I_J \boldsymbol{n}^I_K \boldsymbol{n}^I_R\right). \end{aligned} \tag{13}$$

Note, that for the model considered here, the normal strain components $\boldsymbol{\epsilon}^I_{\text{N}}$ as well as the normal projection tensor $\boldsymbol{N}^I$ are additively decomposed into a normal volumetric and a normal deviatoric part

$$\epsilon^I_{\text{N}} = \epsilon_{\text{V}} + \epsilon^I_{\text{D}}, \quad \boldsymbol{N}^I = \boldsymbol{V} + \boldsymbol{D}^I = \boldsymbol{n}^I \otimes \boldsymbol{n}^I. \tag{14}$$

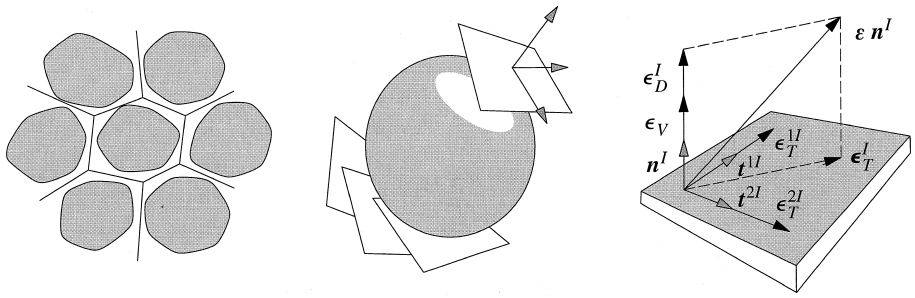

Fig. 1. Microplane kinematics.

The microplane index I has been omitted for the volumetric projection, since the volumetric strain component is identical for each microplane. The projection tensor $\boldsymbol{T}^{RI}$ is of third order for the general three-dimensional case, reducing to a second-order tensor $\boldsymbol{T}^I = \boldsymbol{n}^I \otimes \boldsymbol{t}^I$ with $\boldsymbol{n}^I \cdot \boldsymbol{t}^I = 0$ for a two-dimensional setting. Consequently, the vector of tangential strains $\epsilon_{\mathrm{T}}^{RI}$ reduces to a scalar ϵ_{T}^I for the two-dimensional case.

3.2. Constitutive laws on the microplanes

The constitutive laws for every individual microplane can be formulated based on the theory of plasticity as well as on continuum damage mechanics or a combination of both, see Carol and Bažant [12]. In this study, we will restrict our model to materials for which damage evolution is the dominant dissipative mechanism. The microplane stresses σ_{V}, σ_{D}^I and σ_{T}^{RI} can thus be determined through uniaxial damage laws, given in Lemaitre and Chaboche [19] for example. These damage laws are formulated on every microplane in terms of the individual damage variables d_{V}, d_{D}^I and d_{T}^I and the initial constitutive moduli C_{V}^0,C_{D}^0 and C_{T}^0:

$$\sigma_{\mathrm{V}} = (1 - d_{\mathrm{V}})\ C_{\mathrm{V}}^0 \epsilon_{\mathrm{V}}, \quad \sigma_{\mathrm{D}}^I = (1 - d_{\mathrm{D}}^I) C_{\mathrm{D}}^0 \epsilon_{\mathrm{D}}^I, \quad \sigma_{\mathrm{T}}^{RI} = (1 - d_{\mathrm{T}}^I) C_{\mathrm{T}}^0 \epsilon_{\mathrm{T}}^{RI}. \tag{15}$$

Note, that the tangential damage law is based on the so-called '*parallel tangential hypothesis*' assuming that the tangential stress vector σ_{T}^{RI} always remains parallel to the corresponding strain vector $\epsilon_{\mathrm{T}}^{RI}$. This assumption was first proposed by Bažant and Prat [4] to preserve the one-dimensional character of the constitutive microplane laws also for the tangential law.

As proposed by Lemaitre and Chaboche [19], the damage variables d_{V}, d_{D}^I and d_{T}^I can be interpreted as the reduction of net-stress carrying cross section area fraction of the individual plane

$$d^I = \frac{A_{\mathrm{damaged}}^I}{A_{\mathrm{total}}^I} \quad \text{with } 0 \leqslant d^I \leqslant 1. \tag{16}$$

Herein, A_{damaged}^I defines the effective area of microcracks and microcavities of the Ith microplane, whereas A_{total}^I describes the undamaged microplane area. The evolution of the damage variables is governed by the individual history parameters κ_{V}, κ_{D}^I and κ_{T}^I, representing the most severe deformation in the history of the microplane I:

$$d_{\mathrm{V}} = \hat{d}_{\mathrm{V}}(\kappa_{\mathrm{V}}), \quad d_{\mathrm{D}}^I = \hat{d}_{\mathrm{D}}^I(\kappa_{\mathrm{D}}^I), \quad d_{\mathrm{T}}^I = \hat{d}_{\mathrm{T}}^I(\kappa_{\mathrm{T}}^I). \tag{17}$$

Considering concrete behavior, different laws for tension and compression need to be applied. Bažant and Prat [4] have chosen exponential damage laws except for volumetric compression. They are summarized in Table 1. The resulting stress–strain relations on the individual microplanes are depicted in Fig. 2.

The values of κ are thus nondecreasing. Their growth is only possible, if the corresponding damage loading function $\bar{\Phi}$ is equal to zero. In analogy to the theory of plasticity, the evolution of the history parameters κ is determined by the Kuhn–Tucker conditions:

Table 1
Microplane damage moduli $(1-d)$ for concrete

Volumetric $1-d_{\mathrm{V}}$	Tension $\epsilon_{\mathrm{V}} \geqslant 0$	$\exp\left[-\left[\frac{\kappa_{\mathrm{V}}}{a_1}\right]^{p_1}\right]$
	Compression $\epsilon_{\mathrm{V}} < 0$	$\left[1-\frac{\kappa_{\mathrm{V}}}{a}\right]^{-p}+\left[-\frac{\kappa_{\mathrm{V}}}{b}\right]^{q}$
Deviatoric $1-d_{\mathrm{D}}^{I}$	Tension $\epsilon_{\mathrm{D}}^{I} \geqslant 0$	$\exp\left[-\left[\frac{\kappa_{\mathrm{D}}^{I}}{a_1}\right]^{p_1}\right]$
	Compression $\epsilon_{\mathrm{D}}^{I} < 0$	$\exp\left[-\left[\frac{\kappa_{\mathrm{D}}^{I}}{a_2}\right]^{p_2}\right]$
Tangential $1-d_{\mathrm{T}}^{I}$	Tension $\epsilon_{\mathrm{T}}^{RI} \geqslant 0$	$\exp\left[-\left[\frac{\kappa_{\mathrm{T}}^{I}}{a_3}\right]^{p_3}\right]$
	Compression $\epsilon_{\mathrm{T}}^{RI} < 0$	$\exp\left[-\left[\frac{\kappa_{\mathrm{T}}^{I}}{a_3}\right]^{p_3}\right]$

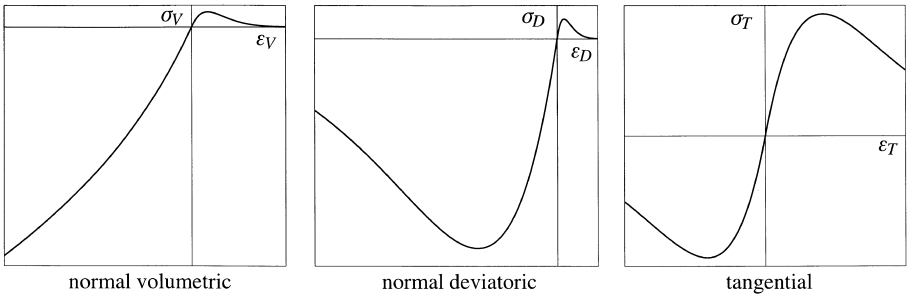

Fig. 2. Individual constitutive laws on a microplane.

$$\begin{aligned} &\dot{\kappa}_{\mathrm{V}} \geqslant 0, \quad \bar{\Phi}_{\mathrm{V}} \leqslant 0, \quad \dot{\kappa}_{\mathrm{V}}\bar{\Phi}_{\mathrm{V}} = 0, \\ &\dot{\kappa}_{\mathrm{D}}^{I} \geqslant 0, \quad \bar{\Phi}_{\mathrm{D}}^{I} \leqslant 0, \quad \dot{\kappa}_{\mathrm{D}}^{I}\bar{\Phi}_{\mathrm{D}}^{I} = 0, \\ &\dot{\kappa}_{\mathrm{T}}^{I} \geqslant 0, \quad \bar{\Phi}_{\mathrm{T}}^{I} \leqslant 0, \quad \dot{\kappa}_{\mathrm{T}}^{I}\bar{\Phi}_{\mathrm{T}}^{I} = 0. \end{aligned} \tag{18}$$

Herein, the damage loading functions $\bar{\Phi}$ are assumed to be formulated in a strain-based fashion in the sense of Simo and Ju [26] ($\bar{\Phi} = \hat{\bar{\Phi}}(\boldsymbol{\epsilon}, \ldots)$). In analogy to gradient plasticity, they also include a gradient term, see de Borst et al. [8]. Thus, the loading functions $\bar{\Phi}$ are assumed to depend not only on the local strains ϵ and on the local history variables κ, but also on the strain gradients $\nabla^2\epsilon$:

$$\bar{\Phi} = \hat{\bar{\Phi}}(\epsilon, \nabla^2\epsilon, \kappa). \tag{19}$$

With the help of Eq. (8), the individual damage loading functions can be written in terms of the absolute value of the nonlocal strains $\bar{\epsilon}$ and the history variables κ.

$$\bar{\Phi}_{\mathrm{V}} = |\bar{\epsilon}_{\mathrm{V}}| - \kappa_{\mathrm{V}} \leqslant 0, \quad \bar{\Phi}_{\mathrm{D}}^{I} = |\bar{\epsilon}_{\mathrm{D}}^{I}| - \kappa_{\mathrm{D}}^{I} \leqslant 0, \quad \bar{\Phi}_{\mathrm{T}}^{I} = \bar{\gamma}_{\mathrm{T}}^{I} - \kappa_{\mathrm{T}}^{I} \leqslant 0. \tag{20}$$

Note, that the tangential loading function is governed by the norm of the corresponding nonlocal tangential strain vector

$$\bar{\gamma}_{\mathrm{T}}^{I} = \sqrt{\bar{\epsilon}_{\mathrm{T}}^{RI}\bar{\epsilon}_{\mathrm{T}}^{RI}} \tag{21}$$

to preserve the one-dimensional format of the tangential microplane laws. The nonlocal strain components of Eq. (20) are defined analogously to their local counterparts, compare with Eq. (12):

$$\bar{\epsilon}_{\mathrm{V}} = \bar{\boldsymbol{\epsilon}} : \boldsymbol{V}, \quad \bar{\epsilon}_{\mathrm{D}}^{I} = \bar{\boldsymbol{\epsilon}} : \boldsymbol{D}^{I}, \quad \bar{\epsilon}_{\mathrm{T}}^{RI} = \bar{\boldsymbol{\epsilon}} : \boldsymbol{T}^{RI}. \tag{22}$$

3.3. Overall constitutive law

The macroscopic stress tensor is related to the microplane stress components by the equivalence of virtual work performed on the surface of a unit sphere. The macroscopic virtual work is given by the scalar product of the stress tensor and the virtual strains integrated over the surface of a unit sphere Ω:

$$\hat{W}^{\text{macro}} = \int_{\Omega} \boldsymbol{\sigma} : \delta\boldsymbol{\epsilon} \, \mathrm{d}\Omega = \frac{4}{3\pi} \boldsymbol{\sigma} : \delta\boldsymbol{\epsilon}. \tag{23}$$

Analogously, the virtual work performed on the microplanes is given by the product of the stress and virtual strain components in the normal and tangential directions integrated over Ω:

$$\hat{W}^{\text{micro}} = \int_{\Omega} ((\sigma_{\text{V}} + \sigma_{\text{D}})\delta\epsilon_{\text{N}} + \sigma_{\text{T}}\delta\epsilon_{\text{T}}) \, \mathrm{d}\Omega. \tag{24}$$

Expressing the virtual strain components $\delta\epsilon_{\text{N}}$ and $\delta\epsilon_T$ through the microplane kinematics of Eq. (12)

$$\delta\epsilon_{\text{N}} = \delta\boldsymbol{\epsilon} : \boldsymbol{N}, \quad \delta\epsilon_{\text{T}} = \delta\boldsymbol{\epsilon} : \boldsymbol{T} \tag{25}$$

and numerically approximating the integral of Eq. (24) by a finite sum yields the overall stress tensor $\boldsymbol{\sigma}$ as a weighted summation of the individual microplane stress components

$$\boldsymbol{\sigma} = \sigma_{\text{V}} \mathbf{1} + \sum_{I=1}^{\text{nmp}} \sigma_{\text{D}}^{I} \boldsymbol{N}^{I} w^{I} + \sum_{I=1}^{\text{nmp}} \sigma_{\text{T}}^{RI} \boldsymbol{T}^{RI} w^{I}. \tag{26}$$

Herein, nmp represents the number of microplanes and w^I are the corresponding weight coefficients. In a two-dimensional setting, 12 microplanes, nmp = 12, of equal weight $w^I = 1/12$ have been shown to yield reasonable results, see for example Bažant and Prat [4]. For a three-dimensional model problem, at least nmp = 21 microplanes should be taken into account, see Stroud [27] for their geometry and the corresponding weight coefficients. The constitutive relation between the macroscopic strain tensor $\boldsymbol{\epsilon}$ and the overall stress tensor $\boldsymbol{\sigma}$ is given through the modified elasticity tensor $\tilde{\boldsymbol{C}}$ which can be interpreted as a summation of the weighted microplane moduli projected by the individual projection tensors:

$$\tilde{\boldsymbol{C}} = (1 - d_{\text{V}}) C_{\text{V}}^{0} \, \mathbf{1} \otimes \boldsymbol{V} + \sum_{I=1}^{\text{nmp}} (1 - d_{\text{D}}^{I}) C_{\text{D}}^{0} \, \boldsymbol{N}^{I} \otimes \boldsymbol{D}^{I} \, w^{I} + \sum_{I=1}^{\text{nmp}} (1 - d_{\text{T}}^{I}) C_{\text{T}}^{0} \, \boldsymbol{T}^{RI} \otimes \boldsymbol{T}^{RI} w^{I}. \tag{27}$$

For the originally undamaged material, $\tilde{\boldsymbol{C}}$ is equal to the elasticity tensor $\boldsymbol{C}^{\text{el}}$, so that C_{V}^{0}, C_{D}^{0} and C_{T}^{0} can be expressed in terms of the Lamé constants μ and λ.

$$\boldsymbol{C}^{\text{el}} = 2\mu \mathbf{1}^{4} + \lambda \mathbf{1} \otimes \mathbf{1} = C_{\text{V}}^{0} \, \mathbf{1} \otimes \boldsymbol{V} + \sum_{I=1}^{\text{nmp}} C_{\text{D}}^{0} \, \boldsymbol{N}^{I} \otimes \boldsymbol{D}^{I} \, w^{I} + \sum_{I=1}^{\text{nmp}} C_{\text{T}}^{0} \, \boldsymbol{T}^{RI} \otimes \boldsymbol{T}^{RI} \, w^{I} = \tilde{\boldsymbol{C}}. \tag{28}$$

Applying the effective stress concept together with the principle of strain equivalence, see [19], the overall stress–strain relation of anisotropic damage can be expressed in terms of the tensor of initial elastic moduli $\boldsymbol{C}^{\text{el}}$ and a fourth-order damage tensor $\boldsymbol{D}$:

$$\boldsymbol{\sigma} = \tilde{\boldsymbol{C}} : \boldsymbol{\epsilon} = (\mathbf{1} - \boldsymbol{D}) : \boldsymbol{C}^{\text{el}} : \boldsymbol{\epsilon}. \tag{29}$$

Consequently, the modified elasticity tensor $\tilde{\boldsymbol{C}}$ which was defined in Eq. (27) can be cast into an overall fourth-order damage tensor:

$$\boldsymbol{D} = \mathbf{1} - \tilde{\boldsymbol{C}} : \boldsymbol{C}^{\text{el}-1}. \tag{30}$$

Thus, the present model fits into the framework of tensorial damage, see Carol et al. [10]. However, there is no need to explicitly calculate this damage tensor $\boldsymbol{D}$. The constitutive equations of the microplane model are summarized in Table 2.

4. Finite element implementation

4.1. Governing equations

The boundary value problem of gradient damage is governed by the equilibrium equation and by the implicit definition of the nonlocal strains:

Table 2
Constitutive equations of the microplane model

Kinematics	$\boldsymbol{\epsilon} = \boldsymbol{\nabla}^{\mathrm{sym}}\boldsymbol{u}$		
Stresses	$\boldsymbol{\sigma} = \boldsymbol{\sigma}_{\mathrm{V}} + \boldsymbol{\sigma}_{\mathrm{D}} + \boldsymbol{\sigma}_{\mathrm{T}}$		
Volumetric	$\boldsymbol{\sigma}_{\mathrm{V}} = \left[(1-d_{\mathrm{V}})C_{\mathrm{V}}^0\,\mathbf{1}\otimes\boldsymbol{V}\right] : \boldsymbol{\epsilon}$		
Deviatoric	$\boldsymbol{\sigma}_{\mathrm{D}}^I = \left[\sum_{I=1}^{\mathrm{nmp}}(1-d_{\mathrm{D}}^I)\,C_{\mathrm{D}}^0\,\boldsymbol{N}^I\otimes\boldsymbol{D}^I\right] : \boldsymbol{\epsilon}$		
Tangential	$\boldsymbol{\sigma}_{\mathrm{T}}^{RI} = \left[\sum_{I=1}^{\mathrm{nmp}}(1-d_{\mathrm{T}}^I)C_{\mathrm{T}}^0\,\boldsymbol{T}^{RI}\otimes\boldsymbol{T}^{RI}\right] : \boldsymbol{\epsilon}$		
Damage			
Volumetric	$d_{\mathrm{V}} = \hat{d}_{\mathrm{V}}(\kappa_{\mathrm{V}})$		
Deviatoric	$d_{\mathrm{D}}^I = \hat{d}_{\mathrm{D}}^I(\kappa_{\mathrm{D}}^I)$		
Tangential	$d_{\mathrm{T}}^I = \hat{d}_{\mathrm{T}}^I(\kappa_{\mathrm{T}}^I)$		
Loading functions			
Volumetric	$\bar{\Phi}_{\mathrm{V}} = \lvert\bar{\epsilon}_{\mathrm{V}}\rvert - \kappa_{\mathrm{V}}$	$\bar{\epsilon}_{\mathrm{V}} = \bar{\boldsymbol{\epsilon}} : \boldsymbol{V}$	
Deviatoric	$\bar{\Phi}_{\mathrm{D}}^I = \lvert\bar{\epsilon}_{\mathrm{D}}^I\rvert - \kappa_{\mathrm{D}}^I$	$\bar{\epsilon}_{\mathrm{D}}^I = \bar{\boldsymbol{\epsilon}} : \boldsymbol{D}^I$	
Tangential	$\bar{\Phi}_{\mathrm{T}}^I = \bar{\gamma}_{\mathrm{T}}^I - \kappa_{\mathrm{T}}^I$	$\bar{\epsilon}_{\mathrm{T}}^{RI} = \bar{\boldsymbol{\epsilon}} : \boldsymbol{T}^{RI}$	$\bar{\gamma}_{\mathrm{T}}^I = \sqrt{\bar{\epsilon}_{\mathrm{T}}^{RI}\,\bar{\epsilon}_{\mathrm{T}}^{RI}}$
Kuhn–Tucker conditions			
Volumetric	$\dot{\bar{\kappa}}_{\mathrm{V}} \geqslant 0$	$\bar{\Phi}_{\mathrm{V}} \leqslant 0$	$\dot{\bar{\kappa}}_{\mathrm{V}}\,\bar{\Phi}_{\mathrm{V}} = 0$
Deviatoric	$\dot{\bar{\kappa}}_{\mathrm{D}}^I \geqslant 0$	$\bar{\Phi}_{\mathrm{D}}^I \leqslant 0$	$\dot{\bar{\kappa}}_{\mathrm{D}}^I\,\bar{\Phi}_{\mathrm{D}}^I = 0$
Tangential	$\dot{\bar{\kappa}}_{\mathrm{T}}^I \geqslant 0$	$\bar{\Phi}_{\mathrm{T}}^I \leqslant 0$	$\dot{\bar{\kappa}}_{\mathrm{T}}^I\,\bar{\Phi}_{\mathrm{T}}^I = 0$

$$\boldsymbol{\nabla}\cdot\boldsymbol{\sigma} + \boldsymbol{f} = \boldsymbol{0}, \tag{31}$$

$$\bar{\boldsymbol{\epsilon}} - c\boldsymbol{\nabla}^2\bar{\boldsymbol{\epsilon}} = \boldsymbol{\epsilon}, \tag{32}$$

where $\boldsymbol{f}$ represents an external load vector. The governing equations can be solved by applying an independent finite element discretization of the displacement field $\boldsymbol{u}$ and the nonlocal strain field $\bar{\boldsymbol{\epsilon}}$. As proposed in Section 2, the following boundary conditions will be applied:

$$\begin{aligned} &\boldsymbol{u} = \boldsymbol{u}^p \quad \text{on } \Gamma_u, \\ &\boldsymbol{t} = \boldsymbol{\sigma}\cdot\boldsymbol{n} \quad \text{on } \Gamma_\sigma, \\ &\bar{\boldsymbol{\epsilon}}_n = \boldsymbol{\nabla}\bar{\boldsymbol{\epsilon}}\cdot\boldsymbol{n} = \boldsymbol{0} \quad \text{on } \Gamma. \end{aligned} \tag{33}$$

Integrating Eqs. (31) and (32) over the domain Ω and weighting with $\boldsymbol{w}_u$ and $\boldsymbol{w}_{\bar{\epsilon}}$, respectively, yields the weak forms given as follows:

$$\int_\Omega \boldsymbol{w}_u^{\mathrm{T}}(\boldsymbol{\nabla}\cdot\boldsymbol{\sigma} + \boldsymbol{f})\,\mathrm{d}\Omega = 0, \tag{34}$$

$$\int_\Omega \boldsymbol{w}_{\bar{\epsilon}}^{\mathrm{T}}(\bar{\boldsymbol{\epsilon}} - c\boldsymbol{\nabla}^2\bar{\boldsymbol{\epsilon}})\,\mathrm{d}\Omega = \int_\Omega \boldsymbol{w}_{\bar{\epsilon}}^{\mathrm{T}}\boldsymbol{\epsilon}\,\mathrm{d}\Omega. \tag{35}$$

Integration by parts, applying the divergence theorem and including the boundary conditions (33) results in the following pair of equations:

$$\int_\Omega \boldsymbol{\nabla}\boldsymbol{w}_u^{\mathrm{T}}\boldsymbol{\sigma}\,\mathrm{d}\Omega = \int_\Omega \boldsymbol{w}_u^{\mathrm{T}}\boldsymbol{f}\,\mathrm{d}\Omega + \int_\Gamma \boldsymbol{w}_u^{\mathrm{T}}\boldsymbol{t}\,\mathrm{d}\Gamma, \tag{36}$$

$$\int_\Omega \boldsymbol{w}_{\bar{\epsilon}}^{\mathrm{T}}\bar{\boldsymbol{\epsilon}}\,\mathrm{d}\Omega + \int_\Omega \boldsymbol{\nabla}\boldsymbol{w}_{\bar{\epsilon}}^{\mathrm{T}}c\boldsymbol{\nabla}\bar{\boldsymbol{\epsilon}}\,\mathrm{d}\Omega = \int_\Omega \boldsymbol{w}_{\bar{\epsilon}}^{\mathrm{T}}\boldsymbol{\epsilon}\,\mathrm{d}\Omega. \tag{37}$$

4.2. Discretization

The corresponding finite element discretization of the displacement field $\boldsymbol{u}$ and the nonlocal strain field $\bar{\boldsymbol{\epsilon}}$ is given by

$$\begin{aligned} \boldsymbol{u} &= \boldsymbol{N}_u \boldsymbol{d}_u, \quad \nabla \boldsymbol{u} = \boldsymbol{B}_u \boldsymbol{d}_u, \\ \bar{\epsilon} &= \boldsymbol{N}_{\bar{\epsilon}} \boldsymbol{d}_{\bar{\epsilon}}, \quad \nabla \bar{\epsilon} = \boldsymbol{B}_{\bar{\epsilon}} \boldsymbol{d}_{\bar{\epsilon}} \end{aligned} \tag{38}$$

with $\boldsymbol{d}_u$ and $\boldsymbol{d}_{\bar{\epsilon}}$ being the nodal degrees of freedom. $\boldsymbol{N}_u$ and $\boldsymbol{N}_{\bar{\epsilon}}$ represent the shape functions and $\boldsymbol{B}_u$ and $\boldsymbol{B}_{\bar{\epsilon}}$ include their partial derivatives with respect to the coordinates. According to the Bubnov-Galerkin method, the corresponding weight functions can be discretized analogously:

$$\begin{aligned} \boldsymbol{w}_u &= \boldsymbol{N}_u \boldsymbol{d}_{wu}, \quad \nabla \boldsymbol{w}_u = \boldsymbol{B}_u \boldsymbol{d}_{wu}, \\ \boldsymbol{w}_{\bar{\epsilon}} &= \boldsymbol{N}_{\bar{\epsilon}} \boldsymbol{d}_{w\bar{\epsilon}}, \quad \nabla \boldsymbol{w}_{\bar{\epsilon}} = \boldsymbol{B}_{\bar{\epsilon}} \boldsymbol{d}_{w\bar{\epsilon}}. \end{aligned} \tag{39}$$

The resulting equations have to be satisfied for all admissible nodal weights $\boldsymbol{d}_{wu}$ and $\boldsymbol{d}_{w\bar{\epsilon}}$. Consequently, the discretized equilibrium equation reduces to

$$\int_\Omega \boldsymbol{B}_u^{\mathrm{T}} \boldsymbol{\sigma} \, \mathrm{d}\Omega = \int_\Omega \boldsymbol{N}_u^{\mathrm{T}} \boldsymbol{f} \, \mathrm{d}\Omega + \int_\Gamma \boldsymbol{N}_u^{\mathrm{T}} \boldsymbol{t} \, \mathrm{d}\Gamma, \tag{40}$$

whereas the discretized implicit definition of the nonlocal strains is given in the following form

$$\int_\Omega (\boldsymbol{N}_{\bar{\epsilon}}^{\mathrm{T}} \boldsymbol{N}_{\bar{\epsilon}} + \boldsymbol{B}_{\bar{\epsilon}}^{\mathrm{T}} c \boldsymbol{B}_{\bar{\epsilon}}) \boldsymbol{d}_{\bar{\epsilon}} \, \mathrm{d}\Omega = \int_\Omega \boldsymbol{N}_{\bar{\epsilon}}^{\mathrm{T}} \boldsymbol{\epsilon} \, \mathrm{d}\Omega. \tag{41}$$

4.3. Linearization

In order to construct a consistent incremental-iterative Newton–Raphson solution procedure, Eqs. (40) and (41) have to be linearized. The main advantage of the gradient continuum equations compared to the nonlocal integral equations is that the linearization is straightforward. At the nodal level, the linearization at iteration i with respect to the previous iteration $i-1$ is given by

$$\boldsymbol{d}_{u,i} = \boldsymbol{d}_{u,i-1} + \Delta \boldsymbol{d}_u, \quad \boldsymbol{d}_{\bar{\epsilon},i} = \boldsymbol{d}_{\bar{\epsilon},i-1} + \Delta \boldsymbol{d}_{\bar{\epsilon}}, \tag{42}$$

which results in the following linearization of the stress tensor at the integration point level:

$$\boldsymbol{\sigma}_i = \boldsymbol{\sigma}_{i-1} + \Delta \boldsymbol{\sigma}. \tag{43}$$

Herein, the incremental stresses $\Delta \boldsymbol{\sigma}$ are given by

$$\Delta \boldsymbol{\sigma} = \left. \frac{\partial \boldsymbol{\sigma}}{\partial \boldsymbol{\epsilon}} \right|_{i-1} : \Delta \boldsymbol{\epsilon} + \left. \frac{\partial \boldsymbol{\sigma}}{\partial \bar{\boldsymbol{\epsilon}}} \right|_{i-1} : \Delta \bar{\epsilon} \tag{44}$$

with the linearized local and nonlocal strain tensor given as follows:

$$\begin{aligned} \boldsymbol{\epsilon}_i &= \boldsymbol{\epsilon}_{i-1} + \Delta \boldsymbol{\epsilon}, \quad \Delta \boldsymbol{\epsilon} = \boldsymbol{B}_u \Delta \boldsymbol{d}_u, \\ \bar{\epsilon}_i &= \bar{\epsilon}_{i-1} + \Delta \bar{\epsilon}, \quad \Delta \bar{\epsilon} = \boldsymbol{N}_{\bar{\epsilon}} \Delta \boldsymbol{d}_{\bar{\epsilon}}. \end{aligned} \tag{45}$$

The partial derivative of the stress tensor with respect to the local strain tensor yields the modified elasticity tensor $\tilde{\boldsymbol{C}}$ which was already defined in Eq. (27):

$$\begin{aligned} \left. \frac{\partial \boldsymbol{\sigma}}{\partial \boldsymbol{\epsilon}} \right|_{i-1} := \tilde{\boldsymbol{C}}_{i-1} = (1 - d_{\mathrm{V},i-1}) C_{\mathrm{V}}^0 \, \boldsymbol{1} \otimes \boldsymbol{V} + \sum_{I=1}^{\mathrm{nmp}} (1 - d_{\mathrm{D},i-1}^I) C_{\mathrm{D}}^0 \, \boldsymbol{N}^I \otimes \boldsymbol{D}^I \, w^I \\ + \sum_{I=1}^{\mathrm{nmp}} (1 - d_{\mathrm{T},i-1}^I) C_{\mathrm{T}}^0 \, \boldsymbol{T}^{RI} \otimes \boldsymbol{T}^{RI} \, w^I. \end{aligned} \tag{46}$$

The following fourth-order tensor which we will denote by $\Delta \tilde{\boldsymbol{C}}$ represents the partial derivative of the stress tensor with respect to the nonlocal strains:

$$\left. \frac{\partial \boldsymbol{\sigma}}{\partial \bar{\boldsymbol{\epsilon}}} \right|_{i-1} := \Delta \tilde{\boldsymbol{C}} = \Delta C_{\mathrm{V}} \, \boldsymbol{1} \otimes \boldsymbol{V} + \sum_{I=1}^{\mathrm{nmp}} \Delta \mathrm{C}_{\mathrm{D}}^{\mathrm{I}} \, \boldsymbol{N}^{\mathrm{I}} \otimes \boldsymbol{D}^{\mathrm{I}} \, \mathrm{w}^{\mathrm{I}} + \sum_{\mathrm{I}=1}^{\mathrm{nmp}} \Delta \mathrm{C}_{\mathrm{T}}^{\mathrm{RS,I}} \, \boldsymbol{T}^{\mathrm{RI}} \otimes \boldsymbol{T}^{\mathrm{SI}} \, \mathrm{w}^{\mathrm{I}}. \tag{47}$$

Herein, ΔC_{V}, ΔC_{D}^I and $\Delta C_{\mathrm{T}}^{RS,I}$ denote the linearization of the individual constitutive moduli on the microplane level:

$$\begin{aligned}
\Delta C_{\mathrm{V}} &= \left[\frac{\partial(1-d_{\mathrm{V}})}{\partial \kappa_{\mathrm{V}}}\right]_{i-1}\left[\frac{\partial \kappa_{\mathrm{V}}}{\partial \bar{\epsilon}_{\mathrm{V}}}\right]_{i-1}\epsilon_{\mathrm{V},i-1}C_{\mathrm{V}}^{0},\\
\Delta C_{\mathrm{D}}^{I} &= \left[\frac{\partial(1-d_{\mathrm{D}}^{I})}{\partial \kappa_{\mathrm{D}}^{I}}\right]_{i-1}\left[\frac{\partial \kappa_{\mathrm{D}}^{I}}{\partial \bar{\epsilon}_{\mathrm{D}}^{I}}\right]_{i-1}\epsilon_{\mathrm{D},i-1}^{I}C_{\mathrm{D}}^{0},\\
\Delta C_{\mathrm{T}}^{RS,I} &= \left[\frac{\partial(1-d_{\mathrm{T}}^{I})}{\partial \kappa_{\mathrm{T}}^{I}}\right]_{i-1}\left[\frac{\partial \kappa_{\mathrm{T}}^{I}}{\partial \bar{\gamma}_{\mathrm{T}}^{I}}\right]_{i-1}\frac{\epsilon_{\mathrm{T},i-1}^{RI}\bar{\epsilon}_{\mathrm{T},i-1}^{SI}}{\bar{\gamma}_{\mathrm{T}}^{I}}C_{\mathrm{T}}^{0}.
\end{aligned} \tag{48}$$

The partial derivatives of the damage moduli according to Bažant and Prat [4] with respect to their history parameters are summarized in Table 3. Since damage growth is only possible for loading, the individual ΔC_{V}, $\Delta C_{\mathrm{D}}^{I}$ and $\Delta C_{\mathrm{T}}^{RS,I}$ reduce to zero for unloading and reloading:

$$\begin{aligned}
\left[\frac{\partial \kappa_{\mathrm{V}}}{\partial \bar{\epsilon}_{\mathrm{V}}}\right]_{i-1} &= \begin{cases} 0 & \text{for} \quad \bar{\Phi}_{\mathrm{V}} \neq 0 \quad \text{(unloading)},\\ 1 & \text{for} \quad \bar{\Phi}_{\mathrm{V}} = 0 \quad \text{(loading)}, \end{cases}\\
\left[\frac{\partial \kappa_{\mathrm{D}}^{I}}{\partial \bar{\epsilon}_{\mathrm{D}}^{I}}\right]_{i-1} &= \begin{cases} 0 & \text{for} \quad \bar{\Phi}_{\mathrm{D}}^{I} \neq 0 \quad \text{(unloading)},\\ 1 & \text{for} \quad \bar{\Phi}_{\mathrm{D}}^{I} = 0 \quad \text{(loading)}, \end{cases}\\
\left[\frac{\partial \kappa_{\mathrm{T}}^{I}}{\partial \bar{\gamma}_{\mathrm{T}}^{I}}\right]_{i-1} &= \begin{cases} 0 & \text{for} \quad \bar{\Phi}_{\mathrm{T}}^{I} \neq 0 \quad \text{(unloading)},\\ 1 & \text{for} \quad \bar{\Phi}_{\mathrm{T}}^{I} = 0 \quad \text{(loading)}. \end{cases}
\end{aligned} \tag{49}$$

Substitution of Eq. (44) into (40) yields the linearized form of the equilibrium equation which takes the familiar form of purely displacement field based finite elements except for the coupling term $\int_{\Omega} \boldsymbol{B}_u^{\mathrm{T}} \Delta\tilde{\boldsymbol{C}} \boldsymbol{N}_{\bar{\epsilon}} \Delta \boldsymbol{d}_{\bar{\epsilon}}\, \mathrm{d}\Omega$ which only occurs for loading:

$$\int_{\Omega} \boldsymbol{B}_u^{\mathrm{T}} \tilde{\boldsymbol{C}}_{i-1} \boldsymbol{B}_u \Delta \boldsymbol{d}_u \,\mathrm{d}\Omega + \int_{\Omega} \boldsymbol{B}_u^{\mathrm{T}} \Delta\tilde{\boldsymbol{C}} \boldsymbol{N}_{\bar{\epsilon}} \Delta \boldsymbol{d}_{\bar{\epsilon}} \,\mathrm{d}\Omega = \int_{\Omega} \boldsymbol{N}_u^{\mathrm{T}} \boldsymbol{f} \,\mathrm{d}\Omega + \int_{\Gamma} \boldsymbol{N}_u^{\mathrm{T}} \boldsymbol{t} \,\mathrm{d}\Gamma - \int_{\Omega} \boldsymbol{B}_u^{\mathrm{T}} \boldsymbol{\sigma}_{i-1} \,\mathrm{d}\Omega. \tag{50}$$

The linearized averaging equation obtained from Eq. (41) by substituting Eq. (45) is given in the following form:

$$\begin{aligned}
&-\int_{\Omega} \boldsymbol{N}_{\bar{\epsilon}}^{\mathrm{T}} \boldsymbol{B}_u \Delta \boldsymbol{d}_u \,\mathrm{d}\Omega + \int_{\Omega} \left(\boldsymbol{N}_{\bar{\epsilon}}^{\mathrm{T}} \boldsymbol{N}_{\bar{\epsilon}} + \boldsymbol{B}_{\bar{\epsilon}}^{\mathrm{T}} c \boldsymbol{B}_{\bar{\epsilon}}\right) \Delta \boldsymbol{d}_{\bar{\epsilon}} \,\mathrm{d}\Omega\\
&\quad = \int_{\Omega} \left((\boldsymbol{N}_{\bar{\epsilon}}^{\mathrm{T}} \boldsymbol{N}_{\bar{\epsilon}} + \boldsymbol{B}_{\bar{\epsilon}}^{\mathrm{T}} c \boldsymbol{B}_{\bar{\epsilon}}) \boldsymbol{d}_{\bar{\epsilon},i-1} - \boldsymbol{N}_{\bar{\epsilon}}^{\mathrm{T}} \boldsymbol{B}_u \boldsymbol{d}_{u,i-1} \right) \mathrm{d}\Omega.
\end{aligned} \tag{51}$$

The governing Eqs. (50) and (51) can be combined in the following system of equations including the enhanced element stiffness matrix, the vector of the unknowns and the external and internal element forces.

Table 3
Linearization of microplane damage moduli $(1-d)$

$\left[\frac{\partial(1-d_{\mathrm{V}})}{\partial \kappa_{\mathrm{V}}}\right]_{i-1}$	Tension $\epsilon_{\mathrm{V}} \geqslant 0$	$-\exp\left[-\left[\frac{\kappa_{\mathrm{V}}}{a_1}\right]^{p_1}\right] p_1 \left[\frac{1}{a_1}\right]^{p_1} [\kappa_{\mathrm{V}}]^{p_1-1}$
	Compression $\epsilon_{\mathrm{V}} < 0$	$-\left[1-\frac{\kappa_{\mathrm{V}}}{a}\right]^{-p-1}\frac{p}{a} + \left[-\frac{\kappa_{\mathrm{V}}}{b}\right]^{q-1}\frac{q}{b}$
$\left[\frac{\partial(1-d_{\mathrm{D}}^{I})}{\partial \kappa_{\mathrm{D}}^{I}}\right]_{i-1}$	Tension $\epsilon_{\mathrm{D}}^{I} \geqslant 0$	$-\exp\left[-\left[\frac{\kappa_{\mathrm{D}}^{I}}{a_1}\right]^{p_1}\right] p_1 \left[\frac{1}{a_1}\right]^{p_1} \left[\kappa_{\mathrm{D}}^{I}\right]^{p_1-1}$
	Compression $\epsilon_{\mathrm{D}}^{I} < 0$	$-\exp\left[-\left[\frac{\kappa_{\mathrm{D}}^{I}}{a_2}\right]^{p_2}\right] p_2 \left[\frac{1}{a_2}\right]^{p_2} \left[\kappa_{\mathrm{D}}^{I}\right]^{p_2-1}$
$\left[\frac{\partial(1-d_{\mathrm{T}}^{I})}{\partial \kappa_{\mathrm{T}}^{I}}\right]_{i-1}$	Tension $\epsilon_{\mathrm{T}}^{RI} \geqslant 0$	$-\exp\left[-\left[\frac{\kappa_{\mathrm{T}}^{I}}{a_3}\right]^{p_3}\right] p_3 \left[\frac{1}{a_3}\right]^{p_3} \left[\kappa_{\mathrm{T}}^{I}\right]^{p_3-1}$
	Compression $\epsilon_{\mathrm{T}}^{RI} < 0$	$-\exp\left[-\left[\frac{\kappa_{\mathrm{T}}^{I}}{a_3}\right]^{p_3}\right] p_3 \left[\frac{1}{a_3}\right]^{p_3} \left[\kappa_{\mathrm{T}}^{I}\right]^{p_3-1}$

$$\begin{bmatrix} \boldsymbol{K}_{uu,i-1} & \boldsymbol{K}_{u\bar{\epsilon},i-1} \\ \boldsymbol{K}_{\bar{\epsilon}u,i-1} & \boldsymbol{K}_{\bar{\epsilon}\bar{\epsilon},i-1} \end{bmatrix} \begin{bmatrix} \Delta \boldsymbol{d}_u \\ \Delta \boldsymbol{d}_{\bar{\epsilon}} \end{bmatrix} = \begin{bmatrix} \boldsymbol{f}_u^{\text{ext}} \\ \boldsymbol{f}_{\bar{\epsilon}}^{\text{ext}} \end{bmatrix} - \begin{bmatrix} \boldsymbol{f}_{u,i-1}^{\text{int}} \\ \boldsymbol{f}_{\bar{\epsilon},i-1}^{\text{int}} \end{bmatrix}. \tag{52}$$

Herein, the submatrices and subvectors are defined as follows:

$$\begin{aligned}
\boldsymbol{K}_{uu,i-1} &= \int_\Omega \boldsymbol{B}_u^{\mathrm{T}} \tilde{\boldsymbol{C}}_{i-1} \boldsymbol{B}_u \, \mathrm{d}\Omega, \\
\boldsymbol{K}_{u\bar{\epsilon},i-1} &= \int_\Omega \boldsymbol{B}_u^{\mathrm{T}} \Delta\tilde{\boldsymbol{C}} \boldsymbol{N}_{\bar{\epsilon}} \, \mathrm{d}\Omega, \\
\boldsymbol{K}_{\bar{\epsilon}u,i-1} &= -\int_\Omega \boldsymbol{N}_{\bar{\epsilon}}^{\mathrm{T}} \boldsymbol{B}_u \, \mathrm{d}\Omega, \\
\boldsymbol{K}_{\bar{\epsilon}\bar{\epsilon},i-1} &= \int_\Omega (\boldsymbol{N}_{\bar{\epsilon}}^{\mathrm{T}} \boldsymbol{N}_{\bar{\epsilon}} + \boldsymbol{B}_{\bar{\epsilon}}^{\mathrm{T}} c \boldsymbol{B}_{\bar{\epsilon}}) \, \mathrm{d}\Omega, \\
\boldsymbol{f}_{u,i-1}^{\text{int}} &= \int_\Omega \boldsymbol{B}_u^{\mathrm{T}} \boldsymbol{\sigma}_{i-1} \, \mathrm{d}\Omega, \\
\boldsymbol{f}_u^{\text{ext}} &= \int_\Omega \boldsymbol{N}_u^{\mathrm{T}} \boldsymbol{f} \, \mathrm{d}\Omega + \int_\Gamma \boldsymbol{N}_u^{\mathrm{T}} \boldsymbol{t} \, \mathrm{d}\Gamma, \\
\boldsymbol{f}_{\bar{\epsilon},i-1}^{\text{int}} &= -\int_\Omega \left((\boldsymbol{N}_{\bar{\epsilon}}^{\mathrm{T}} \boldsymbol{N}_{\bar{\epsilon}} + \boldsymbol{B}_{\bar{\epsilon}}^{\mathrm{T}} c \boldsymbol{B}_{\bar{\epsilon}}) \boldsymbol{d}_{\bar{\epsilon},i-1} - \boldsymbol{N}_{\bar{\epsilon}}^{\mathrm{T}} \boldsymbol{B}_u \boldsymbol{d}_{u,i-1} \right) \mathrm{d}\Omega, \\
\boldsymbol{f}_{\bar{\epsilon}}^{\text{ext}} &= \boldsymbol{0}.
\end{aligned}$$

Note, that the element stiffness matrix of the gradient microplane damage model becomes nonsymmetric since $\boldsymbol{K}_{u\bar{\epsilon}} \neq \boldsymbol{K}_{\bar{\epsilon}u}^{\mathrm{T}}$. After assembling the global system of equations, which is of course nonsymmetric as well, a Newton–Raphson method can be applied to determine the incremental update of the unknowns $\Delta \boldsymbol{d}_u$ and $\Delta \boldsymbol{d}_{\bar{\epsilon}}$.

4.4. Special case of local continuum

The special case of a local continuum can be obtained by setting the gradient parameter c equal to zero. The nonlocal strain tensor thus reduces to the local strain tensor:

$$c = 0 \quad \rightarrow \quad \boldsymbol{\epsilon} = \bar{\boldsymbol{\epsilon}} - c\boldsymbol{\nabla}^2 \bar{\boldsymbol{\epsilon}} = \bar{\boldsymbol{\epsilon}}. \tag{53}$$

For this particular case, the sum of $\tilde{\boldsymbol{C}}$ and $\Delta\tilde{\boldsymbol{C}}$ defines the consistent tangent operator $\tilde{\boldsymbol{C}}^{\text{lin}}$ of the local constitutive model:

$$\tilde{\boldsymbol{C}}^{\text{lin}} = \tilde{\boldsymbol{C}} + \Delta\tilde{\boldsymbol{C}}. \tag{54}$$

The consistent tangent operator can be applied to determine the local loss of ellipticity of the nonenhanced local microplane model, see Kuhl and Ramm [17]. As soon as the singularity of the accoustic tensor $\boldsymbol{q}$,

$$\det \boldsymbol{q} = \det \left[\boldsymbol{n} \tilde{\boldsymbol{C}}^{\text{lin}} \boldsymbol{n} \right] = \boldsymbol{0} \tag{55}$$

is fulfilled for any possible vector $\boldsymbol{n}$, the introduction of a gradient term becomes necessary to avoid the loss of well-posedness of the underlying boundary value problem.

5. Examples

In the following chapter, the capabilities of the present model will be analyzed for several examples. The simulations are based on a set of parameters which have been chosen according to Bažant and Ožbolt [5]. The 10 microplane parameters as well as the two elastic parameters E and ν are summarized in Table 4. In

Table 4
Parameters for the microplane model

E	20 000 N/mm^2
a	0.05
p	1.0
v	0.18
b	0.035
q	1.85
a_1	0.00006
a_2	0.0004
a_3	0.0004
p_1	1.2
p_2	1.1
p_3	1.1

correspondence to the microplane damage laws introduced in Section 3.2, damage evolution in volumetric compression is governed by the parameters a, b, p and q. The parameter sets (a, p) are related to normal tension (a_1, p_1), deviatoric compression (a_2, p_2) and tangential material behavior (a_3, p_3), respectively.

To avoid stress oscillations, it is important to guarantee that the interpolation of the two different fields is balanced. Therefore, we will apply serendipity shape functions for the interpolation of the displacement field $\boldsymbol{u}$ whereas the interpolation of the nonlocal strain field $\bar{\epsilon}$ will be bilinear, see Peerlings et al. [22]. In the following examples, both fields will be integrated numerically by a 2×2 point Gauss integration as indicated in Fig. 3.

5.1. Influence of the gradient enhancement

In the first example, the influence of the gradient term will be investigated. Therefore, a bar of the length $L = 100$ mm will be analyzed under tensile loading. In order to trigger localization, the Young's modulus has been reduced by 5% in a $l = 10$ mm wide zone in the middle of the bar, see Fig. 4. The specimen is discretized with 40, 80 and 160 elements, respectively. Fig. 5 shows the load deflection curves of the three different discretizations (left) as well as the influence of different gradient parameters for the discretization with 80 elements (right). The specimen response is almost identical for the three different discretizations, see Fig. 5 (left). Obviously, due to the incorporation of strain gradients in the loading functions, a mesh-independent solution with a finite energy dissipation has been found. The influence of the gradient parameter c is illustrated in Fig. 5 (right). Obviously, the gradient parameter influences the brittleness of the response. For an increasing gradient parameter, the specimen behaves more ductile and the load-carrying capacity increases. The spreading of the localization zone due to a larger gradient parameter obviously delays the beginning of localization.

The evolution of the local and nonlocal strains corresponding to different gradient parameters is given in Figs. 6 and 7. Five different loading stages are depicted based on a discretization with 80 elements. First, we will analyze the evolution of the local strains presented in Fig. 6 (left). A zone of concentrated straining can already be found after a few load steps. Upon further loading, a clear narrowing of the localization zone is observed. Physically, this behavior can be explained by the coalescence of several microcracks in one single

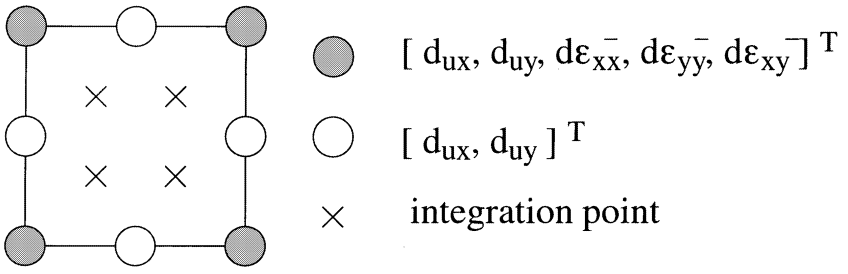

Fig. 3. Degrees of freedom of gradient element.

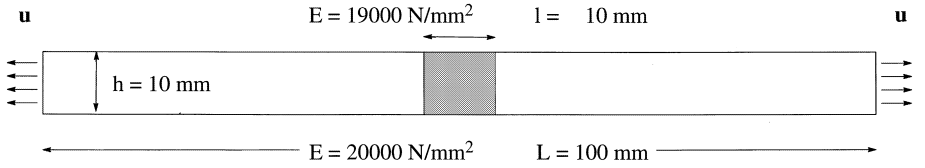

Fig. 4. One-dimensional bar with imperfection – geometry.

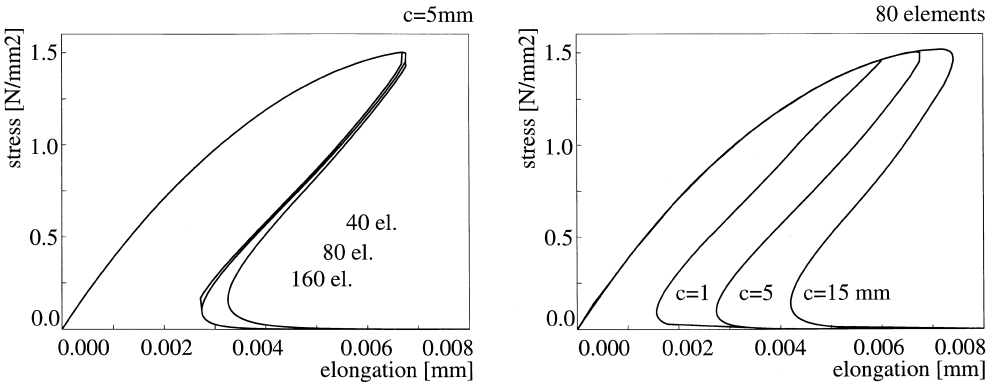

Fig. 5. One-dimensional bar with imperfection – load–deflection curves.

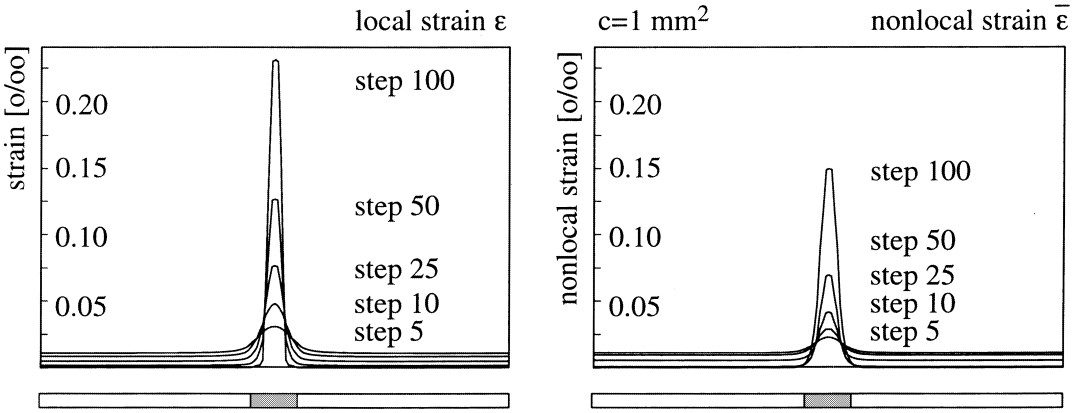

Fig. 6. Evolution of strain distribution in bar with imperfection (1).

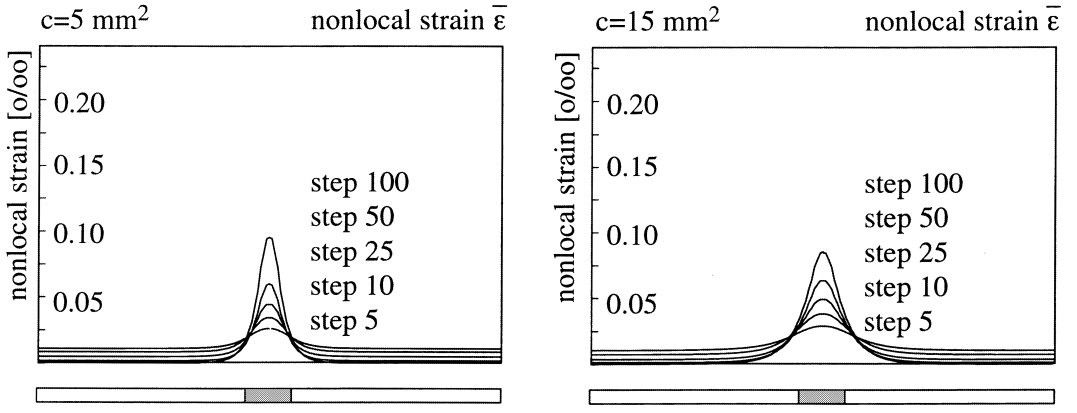

Fig. 7. Evolution of strain distribution in bar with imperfection (2).

macroscopic crack. Nevertheless, the evolution of the nonlocal strains $\bar{\epsilon}$ given in Fig. 6 (right) and Fig. 7 is completely different. The width of concentrated nonlocal strains remains unchanged throughout all steps. Although the amount of the nonlocal strains increases upon further loading, the width of the affected zone is fixed upon initiation. The value of the gradient parameter clearly influences the width of this zone as well as the maximum value of the nonlocal strains in the middle of the bar. When comparing the first loading stage of the four different diagrams in Figs. 6 and 7, almost identical distributions are found. Obviously, the influence of the strain gradients is not yet noticeable at this early stage of loading.

5.2. Localization within a compression panel

The second example concerns compression of a square panel clamped between two rigid platens. The friction coefficients between the loading platens and the specimen are assumed as infinite, thus constraining the lateral movement of those boundaries. The block which is assumed to be in a plane stress state has a thickness of $t = 10$ mm. The gradient parameter has been chosen equal to $c = 20$ mm^2. As indicated in Fig. 8, only one quarter of the system is modelled by 5×5, 10×10 and 15×15 elements, respectively. The corresponding load deflection curves are given in Fig. 8. Since the 5×5 element discretization only represents a rough approximation of the kinematics of the problem, the corresponding load–deflection curve differs slightly from the curves of the finer meshes. However, the curves of the 10×10 and the 15×15 element discretization are almost identical. The regularizing influence of the gradient enhancement is also demonstrated by the three different deformed configurations of Fig. 9 and by the strain distributions given in Fig. 10. Under compressive loading, a clear shear band deformation pattern under an angle of 45° to the loading axis is found.

5.3. Tension specimen with imperfection

Finally, we will analyze the behavior of a specimen under tensile loading. We will investigate one quarter of the system, discretized by 6×12 and 12×24 elements. Again, we have reduced the Young's modulus of the grey element of Fig. 11 by 5%, simulating an imperfection in order to trigger localization. A plane stress situation is assumed. The thickness of the specimen is $t = 10$ mm. Both load–deflection curves are depicted in Fig. 11. In contrast to the compression panel of the previous example, a brittle failure mode is observed for the tension specimen. Furthermore, under compressive loading, the specimen can resist a much higher load than under tensile loading. The characteristic behavior of concrete of being much more sensitive to tension is thus properly reproduced by the microplane model. Subjected to tensile loading, a concrete specimen fails due to decohesion whereas under compressive loading, frictional slip dominates the failure mechanism. When comparing the strain distributions of the compression panel of Fig. 10 with those of the tension specimen of Fig. 12, we observe that this phenomenon is also simulated correctly. In contrast to the

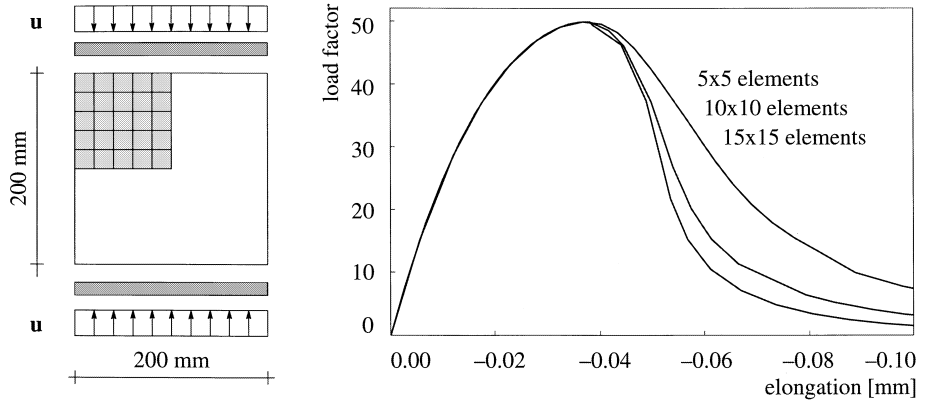

Fig. 8. Geometry and load–deflection curves of compression panel.

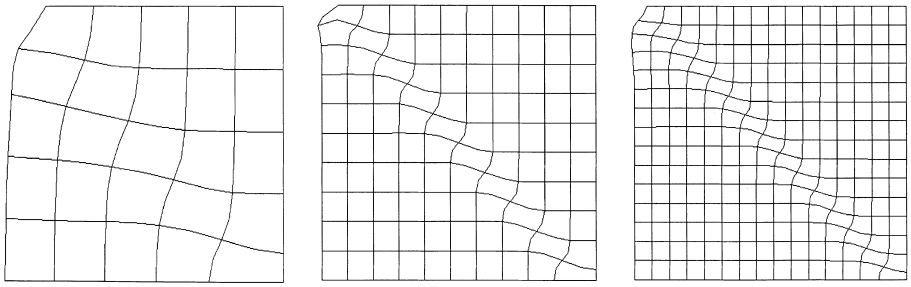

Fig. 9. Deformed configurations on compression panel.

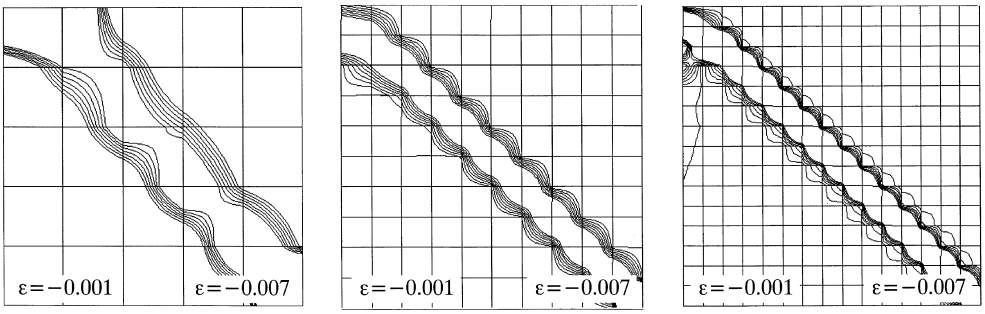

Fig. 10. Strain distributions of compression panel.

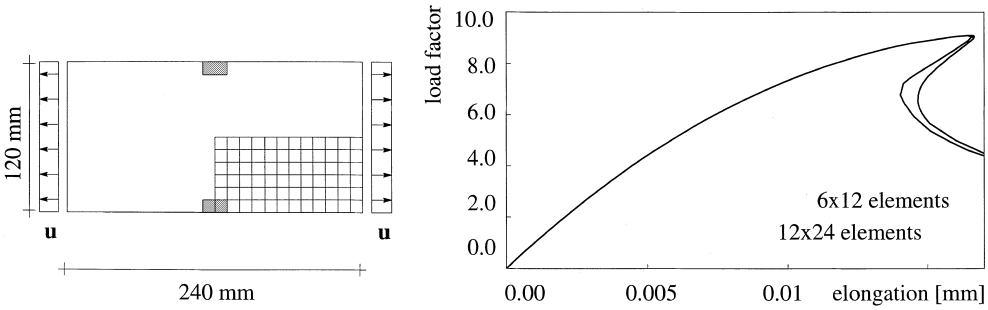

Fig. 11. Geometry and load–deflection curves of tension test.

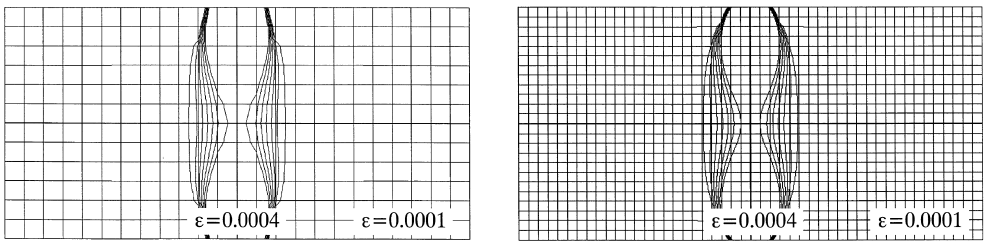

Fig. 12. Strain distributions of tension test.

compression panel, under tensile loading the strains tend to localize in a fracture zone normal to the loading axis as depicted in Fig. 12.

6. Conclusion

A constitutive model for the anisotropic failure of quasi-brittle materials has been developed. Anisotropy has been incorporated via the microplane concept. To account for microstructural interaction, the continuum model has been enriched by strain gradients. Compared to other nonlocal models, the gradient continuum enhancement is considered an elegant way of introducing an internal length scale. The governing equations remain local in a finite element sense and can be solved by introducing an additional field for the gradient term. Consequently, the loss of well-posedness of the boundary value problem is avoided. The influence of the additional gradient term has been investigated by numerical examples which confirmed, that the results remain mesh independent even in the post-critical regime. The presented model thus incorporates in a natural fashion the typical failure mechanisms of quasi-brittle materials, namely failure-induced anisotropy and strain localization.

Acknowledgements

The present study is supported by the Von Humboldt Foundation and the Max Planck Society through the Max Planck Research Award 1996 as well as by grants of the German National Science Foundation (DFG) within the graduate program 'Modellierung und Diskretisierungsmethoden für Kontinua und Strömungen'. This support is gratefully acknowledged.

References

[1] E.C. Aifantis, On the microstructural origin of certain inelastic models, J. Engrg. Mater. Tech. 106 (1984) 326–330.
[2] Z.P. Bažant, P.G. Gambarova, Crack shear in concrete: Crack band microplane model, J. Struc. Engrg. 110 (1984) 2015–2036.
[3] Z.P. Bažant, G. Pijaudier-Cabot, Nonlocal damage, localization instability and convergence, J. Appl. Mech. 55 (1988) 287–293.
[4] Z.P. Bažant, P. Prat, Microplane model for brittle plastic material, I. Theory and II. Verification, J. Engrg. Mech. 114 (1988) 1672–1702.
[5] Z.P. Bažant, J. Ožbolt, Nonlocal microplane model for fracture, damage and size effects in structures, J. Engrg. Mech. 116 (1990) 2485–2505.
[6] Z.P. Bažant, Why continuum damage is nonlocal: micromechanics arguments, J. Engrg. Mech. 117 (1991) 1070–1087.
[7] R. de Borst, H.B. Mühlhaus, Gradient-dependent plasticity: Formulation and algorithmic aspects, Int. J. Numer. Meth. Engrg. 35 (1992) 521–539.
[8] R. de Borst, J. Pamin, R.H.J. Peerlings, L.J. Sluys, On gradient-enhanced damage and plasticity models for failure in quasi-brittle and frictional materials, Comput. Mech. 17 (1995) 130–141.
[9] R. de Borst, A. Benallal, O. Heeres, A gradient-enhanced damage approach to fracture, J. de Physique IV 6 (1996) 491–502.
[10] I. Carol, Z.P. Bažant, P. Prat, Geometric damage tensor based on microplane model, J. Engrg. Mech. 117 (1991) 2429–2448.
[11] I. Carol, P. Prat, Z.P. Bažant, New explicit microplane model for concrete: theoretical aspects and numerical implementation, Int. J. Solids Struc. 29 (1992) 1173–1191.
[12] I. Carol, Z.P. Bažant, Damage and plasticity in microplane theory, Int. J. Solids Struc. 34 (1997) 3807–3835.
[13] A.C. Eringen, D.G.B. Edelen, On nonlocal elasticity, Int. J. Engrg. Science 10 (1972) 233–248.
[14] M.G.D. Geers, Experimental analysis and computational modelling of damage and fracture, Ph.D. Thesis, Eindhoven University of Technology, The Netherlands, 1997.
[15] L.M. Kachanov, On the creep rupture time, Izv. Akad. Nauk SSR, Otd. Tekhn. Nauk 8 (1958) 26–31.
[16] E. Kröner, Elasticity theory of materials with long range cohesive forces, Int. J. Solids Struc. 3 (1967) 731–742.
[17] E. Kuhl, E. Ramm, On the linearization of the microplane model, Mechanics of Cohesive-Frictional Materials 3 (1998) 343–364.
[18] D. Lasry, T. Belytschko, Localization limiters in transient problems, Int. J. Solids Struc. 24 (1988) 581–597.
[19] J. Lemaitre, J.L. Chaboche, Mechanics of Solid Materials, Cambridge University Press, Cambridge, 1990.
[20] H.B. Mühlhaus, E.C. Aifantis, A variational principle for gradient plasticity, Int. J. Solids Struc. 28 (1991) 845–857.
[21] J. Pamin, Gradient-dependent plasticity in numerical simulation of localization phenomena, Ph.D. Thesis, TU Delft, The Netherlands, 1994.
[22] R.H.J. Peerlings, R. de Borst, W.A.M. Brekelmans, J.H.P. de Vree, Gradient-enhanced damage for quasi-brittle materials, Int. J. Numer. Meth. Engrg. 39 (1996) 3391–3403.

[23] R.H.J. Peerlings, R. de Borst, W.A.M. Brekelmans, J.H.P. de Vree, I. Spee, Some observations on localisation in nonlocal and gradient damage models, Eur. J. Mech. A 15 (1996) 937–953.
[24] R.H.J. Peerlings, R. de Borst, W.A.M. Brekelmans, M.G.D. Geers, Gradient enhanced modelling of concrete fracture, Mechanics of Cohesive-Frictional Materials 3 (1998) 323–342.
[25] G. Pijaudier-Cabot, Z.P. Bažant, Nonlocal damage theory, J. Engrg. Mech. 113 (1987) 1512–1533.
[26] J.C. Simo, J.W. Ju, Strain- and stress-based continuum damage models, Int. J. Solids Struc. 23 (1987) 821–869.
[27] A.H. Stroud, Approximate Calculation of Multiple Integrals, Prentice-Hall, Englewood Cliffs, NJ, 1971.
[28] G.I. Taylor, Plastic strain in metals, J. Inst. Metals 62 (1938) 307–324.